IMPACT: International Journal of Research in Applied, Natural and Social Sciences (IMPACT: IJRANSS)
ISSN(P): 2347-4580; ISSN(E): 2321-8851
Vol. 5, Issue 2, Feb 2017, 49-64

QUANTUM CHEMICAL STUDY OF THE RELATIONSHIPS BETWEEN ELECTRONIC STRUCTURE AND ANTIVIRAL ACTIVITIES AGAINST INFLUENZA A H1N1, ENTEROVIRUS 71 AND COXSACKIE B3 VIRUSES OF SOME PYRAZINE-1,3-THIAZINE HYBRID ANALOGUES

JUAN S. GÓMEZ-JERIA[1], PABLO CASTRO-LATORRE[2] & GASTON A. KPOTIN[3]

[1, 2] Quantum Pharmacology Unit, Department of Chemistry, Faculty of Sciences, University of Chile, Las Palmeras, Santiago, Chile

[3]Laboratory of Theoretical Chemistry and Molecular Spectroscopy, Faculty of Sciences and Technique, University of Abomey-Calavi, Cotonou, Benin

ABSTRACT

We have studied the relationships between the electronic structure and the antiviral activity againat H1N1, enterovirus 71 and Coxsackie B3 pathogens. The local atomic reactivity indices were obtained at the B3LYP/6-31G (d,p) level. For two of them (coxsackievirus B3 and H1N1) we obtained statistically significant equations that led to the correponding pharmacophores displaying atomic sites that can be sustituted to obtain molecules endowed with higher inhibitory activity. The results for enterovirus 71 strongly suggest that the molecules seem to have more than one mechanism of action.

KEYWORDS: H1N1, Enterovirus, Coxsackievirus, QSAR, DFT, Influenza

INTRODUCTION

Influenza A (H1N1) virus is the subtype of influenza A virus that was the most common cause of human influenza in 2009 and is associated with the 1918 outbreak that killed 50 to 100 million people. Enterovirus 71 (EV71) is a virus notable for its etiological role in epidemics of severe neurological maladies in children. EV71 occasionally causes polio-like syndrome permanent paralysis. Coxsackie B3 has been found to be one of the chief causes of some weakening or life-threatening maladies, such as viral myocarditis. Several groups of molecules acting again these pathogens have been synthezised and tested (see for example [1-13]).

One of the dreams of a quantum pharmacologist is the opportunity to study a set of molecules having more than one biological action or having a biological effect on different systems. Recently, a group of of pyrazine-1,3-thiazine hybrid analogues was synthezised and tested against influenza A (H1N1) virus, enterovirus 71 (EV71), and coxsackievirus B3 (CVB3) [14]. Given the importance of finding more molecular agents able to combat these pathogens, we presente here the results of the application of a formal method relating the electronic structure with the biological activity for a group of molecules displaying activity against the three abovementioned viruses. of the paper should explain the nature of the problem, previous work, purpose, and the contribution of the paper. The contents of each section may be provided to understand easily about the paper.

METHODS, MODELS AND CALCULATIONS

As the method employed here has been widely discussed in many publications, we refer the reader to the literature [15-21]. Its application to molecule-site binding constants and to other biological activities has produced excellent results [22-49] (and references therein). Therefore, we shall discuss here only the results obtaines from its application. The selected molecules are shown in Figure 1 and Table 1. The biological activities analyzed here (Table 1) are the inhibition of the virus-induced cytopathic effect (CPE) in Madin–Darby canine kidney cells infected with the H1N1 virus (expressed as IC_{50}), and the inhibitory activity against Enterovirus 71 (EV71), expressed as IC_{50}) and coxsackievirus B3 (CVB3, expressed as IC_{50}).

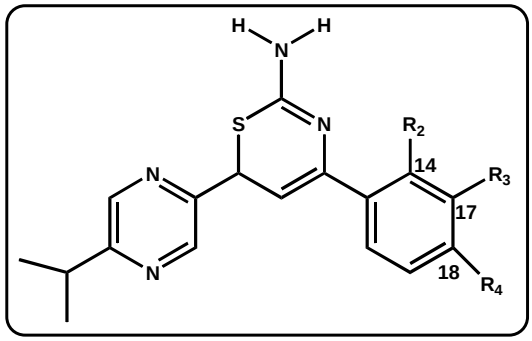

Figure 1: Pyrazine-1, 3-Thiazine Hybrid Analogues

Table 1: Pyrazine-1, 3-Thiazine Hybrid Analogues and Biological Activities

Mol.	Mol.	R_2	R_3	R_4	log(IC_{50}) H1N1	log(IC_{50}) EV71	log(IC_{50}) CVB3
1	3a	H	H	H	1.52	1.19	1.29
2	3b	H	H	OMe	1.05	0.73	1.15
3	3c	H	OMe	H	0.96	0.96	1.05
4	3d	OMe	H	H	0.73	1.25	1.48
5	3e	H	H	Me	1.31	1.05	1.28
6	3f	H	Me	H	1.23	0.95	0.92
7	3g	Me	H	H	1.27	0.35	0.80
8	3h	H	H	OH	1.38	1.26	1.46
9	3i	H	OH	H	1.47	1.21	1.44
10	3j	OH	H	H	1.50	0.39	1.34
11	3k	H	H	NO_2	1.60	1.55	1.26
12	3l	H	NO_2	H	1.65	1.59	1.28
13	3m	NO_2	H	H	1.62	0.82	0.95
14	3n	H	H	Cl	1.73	1.55	1.48
15	3o	H	Cl	H	1.76	1.69	1.59
16	3p	Cl	H	H	1.73	1.74	1.51
17	3q	H	H	F	1.94	1.29	1.53
18	3r	H	F	H	1.97	1.20	1.37
19	3s	F	H	H	-------	1.38	1.62

The electronic structure of all molecules was calculated within the Density Functional Theory (DFT) at the B3LYP/6-31g(d,p) level with full geometry optimization [50]. The Gaussian suite of programs was used [51]. All the information needed to calculate numerical values for the local atomic reactivity indices was obtained from the Gaussian results with the D-Cent-QSAR software [52]. All the electron populations smaller than or equal to 0.01 e were considered

as zero [19]. Negative electron populations coming from Mulliken Population Analysis were corrected as usual [53]. Orientational parameters were taken from the literature [54, 55]. Since the resolution of the system of linear equations is not possible because we have not enough molecules, we made use of Linear Multiple Regression Analysis (LMRA) techniques to find the best solution. For each case, a matrix containing the dependent variable (the log(IC_{50}) of each case) and the local atomic reactivity indices of all atoms of the common skeleton (see below) as independent variables was built. The Statistica software was used for LMRA [56]. We worked with the common skeleton hypothesis stating that there is a definite collection of atoms, common to all molecules analyzed, that accounts for nearly all the biological activity [18]. The action of the substituents consists in modifying the electronic structure of the common skeleton and influencing the right alignment of the drug throughout the orientational parameters. It is hypothesized that different parts or this common skeleton accounts for almost all the interactions leading to the expression of a given biological activity. The common skeleton for this case is shown in Figure 2.

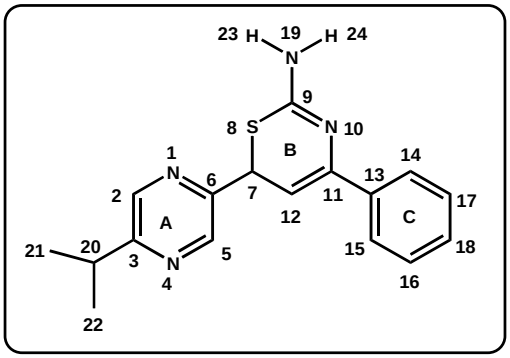

Figure 2: Common Skeleton Numbering

RESULTS

Results for the Inhibition of the Virus-Induced Cytopathic Effect in Madin–Darby Canine Kidney Cells Infected with the H1N1 Virus

The best equation obtained is:

$$\log(IC_{50}) = 2.07 + 0.09S_{11}^{N}(LUMO+2)^{*} - 1.39F_{3}(HOMO-2)^{*} + 1.13F_{16}(LUMO+2)^{*} - 1.07F_{18}(HOMO-2)^{*} + 0.81F_{10}(LUMO+2)^{*} \quad (1)$$

With n=16, R=0.98, R^2=0.97, adj-R^2=0.95, F (5, 10) =58.53 ($p<0.000001$) and a Std. error of estimate of 0.07. No outliers were detected and no residuals fall outside the ±2σ limits. Here, $S_{11}^{N}(LUMO+2)^{*}$ is the nucleophilic superdelocalizability of the third lowest empty MO localized on atom 11, $F_3(HOMO-2)^{*}$ is the Fukui index of the third highest occupied MO localized on atom 11, $F_{16}(LUMO+2)^{*}$ is the Fukui index of the third lowest empty MO localized on atom 16, $F_{18}(HOMO-2)^{*}$ is the Fukui index of the third highest occupied MO localized on atom 18 and $F_{10}(LUMO+2)^{*}$ is the Fukui index of the third lowest empty MO localized on atom 10. Tables 2 and 3 show the beta coefficients, the results of the t-test for significance of coefficients and the matrix of squared correlation coefficients for the variables of Eq. 1. There are no significant internal correlations between independent variables (Table 3). Figure 3 displays the plot of observed *vs.* calculated log (IC_{50}).

Table 2: Beta Coefficients and t-Test for Significance of Coefficients in Eq. 1

Variable	Beta	t(10)	p-level
S_{11}^{N}(LUMO+2)*	0.88	10.95	<0.000001
F_3(HOMO-2)*	-0.37	-5.38	<0.0003
F_{16}(LUMO+2)*	0.56	7.86	<0.00001
F_{18}(HOMO-2)*	-0.27	-3.94	<0.003
F_{10}(LUMO+2)*	0.16	2.74	<0.02

Table 3: Matrix of Squared Correlation Coefficients for the Variables in Eq. 1

	S_{11}^{N}(LUMO+2)*	F_3(HOMO-2)*	F_{16}(LUMO+2)*	F_{18}(HOMO-2)*
F_3(HOMO-2)*	0.20	1		
F_{16}(LUMO+2)*	0.22	0.05	1	
F_{18}(HOMO-2)*	0.03	0.05	0.06	1
F_{10}(LUMO+2)*	0.01	0.02	0.02	0.01

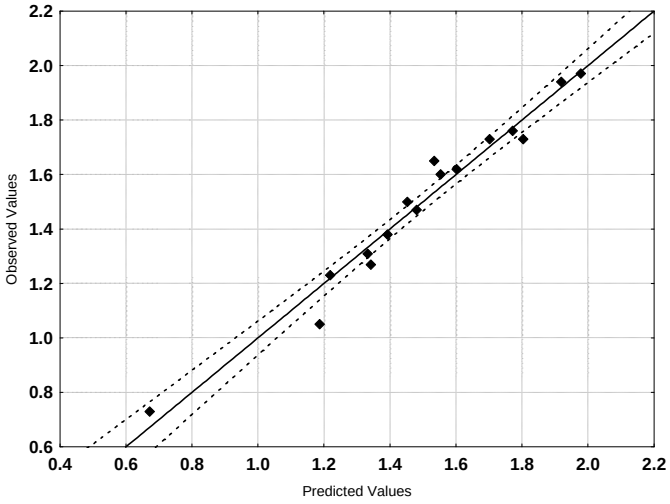

Figure 3: Plot of Predicted *Vs*. Observed Log (IC_{50}) Values (Eq. 1). Dashed Lines Denote the 95% Confidence Interval

The associated statistical parameters of Eq. 1 indicate that this equation is statistically significant and that the variation of the numerical values of a group of five local atomic reactivity indices of atoms of the common skeleton explains about 95% of the variation of log (IC_{50}). Figure 3, spanning about 1.4 orders of magnitude, shows that there is a good correlation of observed *versus* calculated values.

Results for the Inhibition of Enterovirus 71 (EV71)

The best equation obtained is:

$$\log(IC_{50})=-49.83+0.23S_{24}^{N}(LUMO+2)^{*}-0.006S_{13}^{N}(LUMO+2)^{*}-84.71Q_{19} \quad \textbf{(2)}$$

With n=19, R=0.96, R^2=0.92, Adj-R^2=0.91, F (3, 15) =59.932 (p<0.000001) and a Std. error of estimate of 0.12. No outliers were detected and no residuals fall outside the ±2σ limits. Here, S_{24}^{N}(LUMO+2)* is the nucleophilic superdelocalizability of the third lowest empty MO localized on atom 24, S_{13}^{N}(LUMO+2)* is the nucleophilic superdelocalizability of the third lowest empty MO localized on atom 13 and Q_{19} is the net charge of atom 19. Tables 4 and 5 show the beta coefficients, the results of the t-test for significance of coefficients and the matrix of squared correlation

coefficients for the variables of Eq. 2. There are no significant internal correlations between independent variables (Table 7). Figure 4 displays the plot of observed *vs.* calculated log (IC_{50}).

Table 4: Beta Coefficients and t-Test for Significance of Coefficients in Eq. 2

Variable	Beta	t(15)	p-level
S_{24}^{N}(LUMO+2)*	0.73	9.78	<0.000000
S_{13}^{N}(LUMO+2)*	-0.56	-7.30	<0.000003
Q_{19}	-0.25	-3.22	<0.006

Table 5: Matrix of Squared Correlation Coefficients for the Variables in Eq. 2

	S_{24}^{N}(LUMO+2)*	S_{13}^{N}(LUMO+2)*
S_{13}^{N}(LUMO+2)*	0.05	1
Q_{19}	0.05	0.11

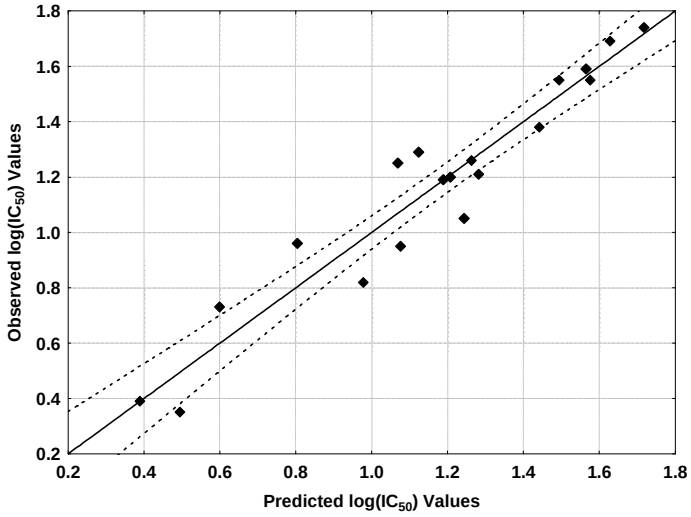

Figure 4: Plot of Predicted *Vs.* Observed Log (IC_{50}) Values (Eq. 2). Dashed Lines Denote the 95% Confidence Interval

The associated statistical parameters of Eq. 2 indicate that this equation is statistically significant and that the variation of the numerical values of a group of three local atomic reactivity indices of atoms of the common skeleton explains about 91% of the variation of log (IC_{50}). Figure 4, spanning about 1.3 orders of magnitude, shows that there is a good correlation of observed *versus* calculated values.

Results for the Inhibition of Coxsackievirus B3 (CVB3)

The best equation obtained is:

$$\log(IC_{50})=57.98+0.40S_{18}^{E}(\text{HOMO-2})^{*}-1.10F_{17}(\text{LUMO+2})^{*}-0.10S_{24}^{N}(\text{LUMO+1})^{*}-$$
$$-4.84Q_{16}+125.91Q_{2}+0.28Q_{14} \quad \textbf{(3)}$$

With n=19, R=0.97 R^2=0.94, adj-R^2=0.91, F(6,12)=29.649 (p<0.00001) and a Std. error of estimate of 0.07. No outliers were detected and no residuals fall outside the ±2σ limits. Here, S_{18}^{E} (HOMO-2)* is the electrophilic superdelocalizability of the third highest occupied MO localized on atom 18, F_{17} (LUMO+2)* is the Fukui index of the third lowest empty MO localized on atom 17, S_{24}^{N} (LUMO+1)* is the nucleophilic superdelocalizability of the second

lowest MO localized on atom 24, Q_{16} is the net charge of atom 16, Q_2 is the net charge of atom 2 and Q_{14} is the net charge of atom 14. Tables 6 and 7 show the beta coefficients, the results of the t-test for significance of coefficients and the matrix of squared correlation coefficients for the variables of Eq. 3. There are no significant internal correlations between independent variables (Table 7). Figure 5 displays the plot of observed *vs.* calculated log (IC_{50}).

Table 6: Beta Coefficients and t-Test for Significance of Coefficients in Eq. 3

Variable	Beta	t(12)	p-level
S_{18}^{E}(HOMO-2)*	0.55	6.16	<0.00004
F_{17}(LUMO+2)*	-0.63	-6.85	<0.00002
S_{24}^{N}(LUMO+1)*	-0.46	-5.46	<0.0001
Q_{16}	-0.36	-3.40	<0.005
Q_2	0.40	3.66	<0.003
Q_{14}	0.21	2.23	<0.05

Table 7: Matrix of Squared Correlation Coefficients for the Variables in Eq. 3

	S_{18}^{E}(HOMO-2)*	F_{17}(LUMO+2)*	S_{24}^{N}(LUMO+1)*	Q_{16}	Q_2
F_{17}(LUMO+2)*	0.04	1			
S_{24}^{N}(LUMO+1)*	0.04	0.11	1		
Q_{16}	0.14	0.31	0.23	1	
Q_2	0.20	0.12	0.13	0.31	1
Q_{14}	0.00	0.00	0.08	0.10	0.25

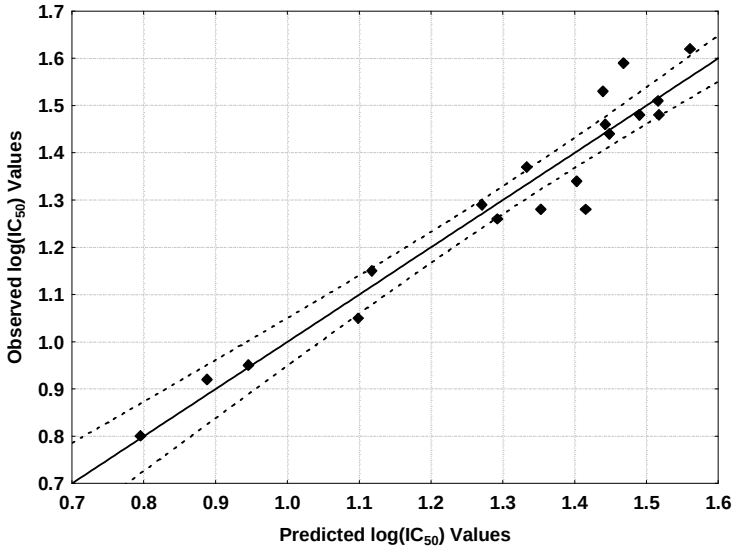

Figure 5: Plot of Predicted *Vs.* Observed Log (IC_{50}) Values (Eq. 3). Dashed Lines Denote the 95% Confidence Interval

The associated statistical parameters of Eq. 3 indicate that this equation is statistically significant and that the variation of the numerical values of a group of six local atomic reactivity indices of atoms of the common skeleton explains about 91% of the variation of log (IC_{50}). Figure 5, spanning about 0.8 orders of magnitude, shows that there is a good correlation of observed *versus* calculated values.

LOCAL MOLECULAR ORBITALS

TABLES 8 TO 10 SHOW THE LOCAL MO STRUCTURE OF ATOMS 2-4, 10-13, 16-18, 20, 23 AND 24 (SEE FIGURE 2). NOMENCLATURE: MOLECULE (HOMO) / (HOMO-2)* (HOMO-1)* (HOMO)* - (LUMO)* (LUMO+1)* (LUMO+2)*.

Table 8: Local Molecular Orbitals of Atoms 2, 3, 4 and 10

Mol.	Atom 2	Atom 3	Atom 4	Atom 10
1(82)	80σ81σ82σ-83π84π85π	79σ80σ81σ-83π85π87π	80σ81σ82σ-83π84π87π	80π81π82π-83σ84π86π
2(90)	85π86π88σ-91π92π93π	85π86π88σ-91π92π93π	88σ89σ90σ-91π92π95π	88π89π90π-91π92π94π
3(90)	86π87σ88σ-91π92π93π	86π87σ88σ-91π92π93π	88σ89σ90σ-91π92π95π	88σ89π90π-91π92π94π
4(90)	86π87σ88σ-91π92π93π	86π87σ88σ-91π92π93π	87σ88σ90σ-91π92π93π	88σ89π90π-91π92π93π
5(86)	84σ85σ86σ-87π88π89π	83σ84σ85σ-87π88π89π	84σ85σ86σ-87π88π91π	84σ85σ86π-87π88π90π
6(86)	83σ84σ86σ-87π88π89π	82π83σ84σ-87π88π89π	84σ85σ86σ-87π88π91π	84π85π86π-87π88π90π
7(86)	83σ84σ86σ-87π88π89π	82π83σ84σ-87π88π 89π	84σ85σ86σ-87π88π 89π	84π85π86π-87π88π 89π
8(86)	81π82π84σ-87π88π89π	81π82π84σ-87π88π89π	84σ85σ86σ-87π88π91π	84π85π86π-87π88π91π
9(86)	82π83σ84σ-87π88π89π	82π83σ84σ-87π88π89π	84σ85σ86σ-87π88π91π	84π85π86π-87π88π90π
10(86)	83σ84σ86σ-87π88π89π	82π83σ84σ-87π88π89π	83σ84σ86σ-87π88π89π	84π85π86π-87π88π89σ
11(93)	91σ92σ93σ-95π96π97π	90π91σ92σ-95π96π97π	91σ92σ93σ-95π96π100π	90π91π93π-95π96π97π
12(93)	91σ92σ93σ-95π96π97π	90π91σ92σ-95π96π97π	91σ92σ93σ-95π96π97π	90π91π93π-95π96π97π
13(93)	91π92σ93σ-95π96π97π	90π91π92σ-95π96π97π	91π92σ93σ-95π96π97π	91π92π93σ-95π96π97π
14(90)	88σ89σ90σ-91π92π93π	87π88σ89σ-91π93π95π	88σ89σ90σ-91π92π93π	88π89π90π-91π92π94π
15(90)	88σ89σ90σ-91π92π93π	87σ88σ89σ-91π93π95π	88σ89σ90σ-91π92π93π	88π89π90π-91π92π94π
16(90)	88σ89σ90σ-91π92π93π	87π88σ89σ-91π92π93π	88σ89σ90σ-91π92π96π	87π89π90π-91π92π94π
17(86)	84σ85σ86σ-87π88π89π	83π84σ85σ-87π89π91π	84σ85σ86σ-87π88π91π	84σ85π86π-87π88π91π
18(86)	84σ85σ86σ-87π88π89π	83σ84σ85σ-87π89π90π	84σ85σ86σ-87π88π91π	84σ85σ86π-87π88π90π
19(86)	84σ85σ86σ-87π88π89π	83π84σ85σ-87π88π89π	84σ85σ86σ-87π88π92π	84π85π86π-87π88π90π

Table 9: Local Molecular Orbitals of Atoms 11, 12, 13 and 16

Mol.	Atom 11	Atom 12	Atom 13	Atom 16
1(82)	76σ77σ82π-83π 84π85π	77σ79σ82π-83π 84π85π	80π81π82π-83π 84π85π	80π81π82π-86π90π91π
2(90)	88π89π90π-91π92π93π	88π89π90π-91π92π93π	87π89π90π-92π93π94π	88π89π90π-94π98π99π
3(90)	86π89π90π-91π92π93π	87π89π90π-91π92π93π	87π88σ90π-91π92π93π	87π88σ89π-93π94π95π
4(90)	88π89π90π-91π92π93π	88π89π90π-91π92π93π	88π89π90π-92π93π94π	88π89π90π-93π95π96π
5(86)	82π83π86π-87π88π89π	83π85σ86π-87π88π89π	83π85π86π-87π88π89π	84π85π86π-90π94π95π
6(86)	81σ82π86π-87π88π89π	83π85π86π-87π88π89π	84π85π86π-87π88π89π	83π84π85π-89π90π94π
7(86)	82π83π86π-87π88π89π	83π85σ86π-87π88π89π	84π85π86π-88π89π90π	84π85π86π-89π90π91π
8(86)	84π85π86π-87π88π89π	84π85π86π-87π88π89π	84π85π86π-88π89π90π	84π85π86π-90π91π95π
9(86)	82π85π86π-87π88π89π	83π85π86π-87π88π89π	83π84π86π-87π88π89π	83π84π85π-89π90π91π
10(86)	84π85π86π-87π88π89π	84π85π86π-87π88π89π	84π85π86π-88π89π90π	84π85π86π-89π90π91π
11(93)	91π92π93π-94π95π96π	90σ92π93π-94π95π96π	91π92π93π-94π97π98π	89π90π91π-94π95π96π
12(93)	91π92π93π-94π95π96π	90σ92π93π-94π95π96π	91π92π93π-94π95π96π	89π90π91π-94π95π96π
13(93)	91π92π93π-94π95π96π	90σ92π93π-94π95π96π	89π90π91π-94π95π96π	88π89π90π-94π98π99π
14(90)	85σ87π90π-91π92π93π	86σ88π90π-91π92π93π	88π89π90π-91π92π93π	88π89π90π-93π94π95π
15(90)	85σ88π90π-91π92π93π	85σ88π90π-91π92π93π	88π89π90π-91π92π93π	87π88π89π-93π94π97σ
16(90)	86σ87π90π-91π92π93π	86σ88π90π-91π92π93π	87π89π90π-91π92π93π	88π89π90π-92π93π94π
17(86)	81σ83π86π-87π88π89π	82σ84π86π-87π88π89π	84π85π86π-87π88π89π	84π85π86π-90π91π94π
18(86)	81σ84π86π-87π88π89π	83π84π86π-87π88π89π	84π85π86π-87π88π89π	83π84π85π-89π90π91π
19(86)	82σ83π86π-87π88π89π	82σ84π86π-87π88π89π	83π85π86π-87π88π89π	84π85π86π-89π90π91π

Table 10: Local Molecular Orbitals of Atoms 17, 18, 20 and 24

	Atom 17	Atom 18	Atom 20	Atom 23	Atom 24
1(82)	79π80π82π-84π85π86π	80π81π82π-83π84π85π	78σ79σ80σ-83σ95σ96σ	50σ52σ53σ-87σ88σ89σ	63σ64σ77σ-89σ90σ91σ
2(90)	87π89π90π-92π93π94π	87π89π90π-91π92π93π	84σ86σ88σ-91σ104σ105σ	55σ56σ59σ-95σ96σ97σ	61σ70σ85σ-97σ98σ99σ
3(90)	8389π90π-92π93π94π	88π89π90π-91π92π93π	84σ86σ87σ-91σ104σ105σ	53σ54σ60σ-94σ95σ96σ	70σ84σ85σ-97σ98σ99σ
4(90)	88π89π90π-93π94π95π	88π89π90π-91π92π93π	86σ87σ88σ-91σ104σ105σ	55σ57σ60σ-92σ94σ96σ	70σ71σ85σ-97σ98σ99σ
5(86)	84π85π86π-88π89π90π	83π85π86π-87π88π89π	82σ83σ84σ-87σ99σ100σ	50σ52σ54σ-91σ92σ93σ	57σ66σ81σ-93σ94σ95σ
6(86)	83π85π86π-88π89π90π	84π85π86π-87π88π89π	80σ82σ83σ-87σ99σ100σ	50σ52σ54σ-91σ92σ93σ	66σ67σ81σ-93σ94σ95σ

Table 10: Contd					
7(86)	83π84π85π-89π90π91π	84π85π86π-87π88π89π	82σ83σ84σ-87σ99σ101σ	52σ55σ56σ-88σ90σ92σ	66σ67σ81σ-93σ94σ95σ
8(86)	83π85π86π-88π89π90π	82π85π86π-87π88π89π	80σ82σ84σ-87σ100σ101σ	51σ53σ54σ-91σ92σ93σ	61σ67σ81σ-93σ94σ95σ
9(86)	76σ85π86π-88π89π90π	84π85π86π-87π88π89π	82σ83σ84σ-87σ100σ101σ	52σ55σ57σ-90σ91σ92σ	67σ80σ81σ-93σ94σ95σ
10(86)	84π85π86π-89π90π91π	84π85π86π-87π88π89π	80σ83σ84σ-87σ99σ100σ	52σ53σ57σ-88σ90σ92σ	67σ69σ81σ-93σ94σ95σ
11(93)	87π88π89π-94π97π98π	91π92π93π-94π97π98π	90σ91σ92σ-95σ107σ108σ	57σ59σ60σ-96σ99σ100σ	70σ72σ87σ-101σ102σ103σ
12(93)	88π89π93π-94π98π99π	91π92π93π-94π95π96π	90σ91σ92σ-95σ107σ108σ	57σ61σ63σ-98σ99σ100σ	65σ70σ72σ-101σ102σ103σ
13(93)	88π89π90π-94π95π96π	90π91π93π-94π95π96π	90σ91σ92σ-95σ107σ108σ	59σ61σ63σ-95σ99σ100σ	70σ72σ87σ-101σ102σ103σ
14(90)	87π89π90π-91π92π93π	88π89π90π-91π92π93π	84σ87σ88σ-91σ103σ104σ	56σ58σ61σ-95σ96σ98σ	70σ84σ85σ-98σ99σ100σ
15(90)	88π89π90π-91π92π93π	87π89π90π-91π92π93π	87σ88σ89σ-91σ103σ104σ	55σ56σ58σ-95σ96σ98σ	62σ70σ84σ-98σ99σ100σ
16(90)	87π88π89π-93π94π97σ	87π89π90π-91π92π93π	84σ87σ88σ-91σ104σ105σ	58σ60σ70σ-92σ95σ96σ	66σ70σ86σ-98σ99σ100σ
17(86)	83π85π86π-88π89π90π	84π85π86π-87π88π89π	80σ83σ84σ-87σ99σ100σ	53σ56σ58σ-91σ92σ93σ	67σ80σ81σ-93σ94σ95σ
18(86)	84π85π86π-88π89π90π	84π85π86π-87π88π89π	82σ83σ84σ-87σ99σ100σ	52σ53σ57σ-90σ91σ92σ	67σ80σ81σ-93σ94σ95σ
19(86)	83π84π85π-89π90π91π	83π85π86π-87π88π89π	80σ83σ84σ-87σ99σ100σ	52σ53σ57σ-90σ91σ92σ	67σ69σ81σ-93σ94σ95σ

DISCUSSIONS

A Equations 1-3 show that there is a linear relationship between the variation of the biological property (log (IC_{50})) and the variation of the numerical values of a definite set of local atomic reactivity indices. In the following we shall discuss case by case.

Discussion of the results for the inhibition of the virus-induced cytopathic effect in Madin–Darby canine kidney cells infected with the H1N1 virus.

Table 2 shows that the importance of variables in Eq. 1 is S_{11}^{N} (LUMO+2)*>> F_{16} (LUMO+2)*> F_3 (HOMO-2)*> F_{18} (HOMO-2)*> F_{10} (LUMO+2)*. Eq. 1 shows that a high inhibitory activity is associated with large numerical values for F_3 (HOMO-2)* and F_{18} (HOMO-2)*, and with small numerical values for F_{16} (LUMO+2)* and F_{10} (LUMO+2)*. As S_{11}^{N} (LUMO+2)* is negative, then a high inhibitory activity is associated with large numerical values for this index. Atom 11 is a carbon in ring A (Figure 2). $(LUMO)_{11}$*, $(LUMO+1)_{11}$* and $(LUMO+2)_{11}$* are π MOs (Table 9). Large negative values for S_{11}^{N} (LUMO+2)* are obtained by shifting upwards the $(LUMO+2)_{11}$* eigenvalue. Therefore, a good inhibitory activity is associated with empty MOs with low reactivity. This suggests that atom 11 is interacting as an electron donor. Atom 16 is a carbon in ring C (Figure 2). $(LUMO+2)_{16}$*, $(LUMO+1)_{16}$* and $(LUMO)_{16}$* have a π nature (Table 9). From Table 9 we can observe that $(LUMO)_{16}$* does not coincide with the molecule's LUMO. As a low value for F_{16} (LUMO+2)* is associated with a high inhibitory activity, a molecule with its five or six lowest empty MOs are not localized on atom 16 will be a good candidate. This suggests that atom 16 is interacting as an electron donor. Atom 3 is a

carbon in ring A (Figure 2). Large numerical values of F_3(HOMO-2)* are associated with high inhibitory activity (let us remember that the values of the Fukui indices are in the [0,2] interval). Table 8 shows that $(HOMO-2)_3$*, $(HOMO-1)_3$* and $(HOMO)_3$* have π or σ natures. This is a direct effect of the isopropyl substituent. The only way to integrate these facts is by suggesting that atom 3 could interact with two sites, one having π MOs and the other σ MOs. Atom 18 is a carbon in ring C (Fig. 2). Large numerical values for F_{18} (HOMO-2)* are associated with a high inhibitory activity. $(HOMO-2)_{18}$*, $(HOMO-1)_{18}$* and $(HOMO)_{18}$* have a π nature (Table 10). This suggests that atom 18 is acting as an electron donor. Atom 10 is nitrogen in ring B (Figure 2). A high inhibitory activity is associated with small numerical values for F_{10} (LUMO+2)*. Almost all $(LUMO)_{10}$* have a π nature, all $(LUMO+1)_{10}$* have a π nature and almost all $(LUMO+1)_{10}$* have a π nature (Table 8). In quantum-chemical calculations of complex molecules like these ones, it is unavoidable that one or more empty MOs be localized on this atom. In this case we suggest the ideal situation is when the lowest empty local MOs do not correspond to the lowest empty MOs of the molecule. Regarding this point, it is suggested that quantum-chemical calculations be made with different substituents at position 12 (Figure 2) to examine their effects on the localization of the empty MOs on atom 10. Within the framework, it seems that atom 10 is acting as an electron donor. All the suggestions are displayed in the partial 2D pharmacophore of Figure 6.

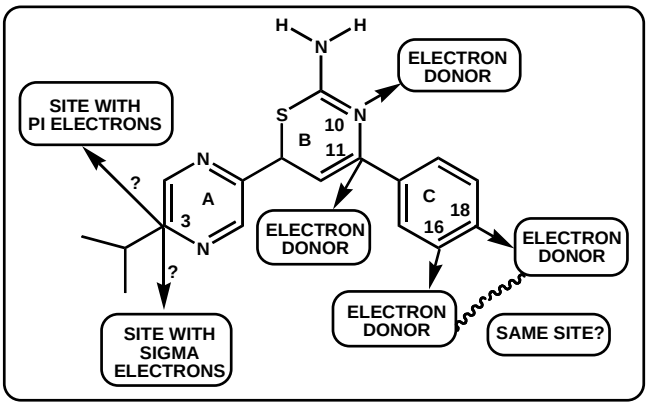

Figure 6: Partial 2D Pharmacophore for the Inhibition of the Virus-Induced Cytopathic Effect in Madin–Darby Canine Kidney Cells Infected with the H1N1 Virus

Discussion of the Results for the Inhibition of Enterovirus 71 (EV71)

Figure 4 shows that several points are outside the 95% confidence interval. A possible explanation is that an unknown factor has not been considered. Therefore, the following analysis must be taken with caution. Table 4 shows that the importance of variables in Eq. 2 is S_{24}^N (LUMO+2)*> S_{13}^N (LUMO+2)*>> Q_{19}. A high inhibitory activity is associated with a low negative net charge on atom 19. If S_{24}^N (LUMO+2)* is positive, a high inhibitory activity is associated with small numerical values for this index. If S_{13}^N (LUMO+2)* is positive, a high activity is associated with large numerical values. Atom 19 is the nitrogen of the NH_2 group attached to ring B. The requirement of a low negative net charge can be understood by suggesting that this atom is participating in a hydrogen bond of the form N-H...X, where X is an atom less electronegative that N or it is participating in an H-bond acceptor through its lone pairs. Atom 24 is one of the hydrogen atoms bonded to the abovementioned NH_2 group. Table 10 shows, as expected, that all occupied and empty local MOs are very far from the molecule's frontier MOs. All they have a σ nature (Table 10). Small positive numerical values for S_{24}^N(LUMO+2)* are associated with a high inhibitory activity. Low values are obtained by moving upwards the energy of

the associated eigenvalue, making this MO less reactive. The plot of S_{24}^{N} (LUMO)* *vs.* log (IC_{50}) (not shown) shows the same trend. The only explanation we have for these facts is that this H atom is facing a region with empty σ MOs and it is engaged in a repulsive interaction with them (zero electrons). Atom 13 is the carbon in ring C (Figure 2). A high inhibitory activity is associated with large positive values of S_{13}^{N} (LUMO+2)*. Table 9 shows that the three lowest empty local MOs have a π nature. Large positive values are obtained by shifting downwards the energy of the corresponding eigenvalue, making this MO more reactive. Therefore, we suggest that atom 13 seems to act as an electron acceptor. All the suggestions are displayed in the partial 2D pharmacophore of Figure 7.

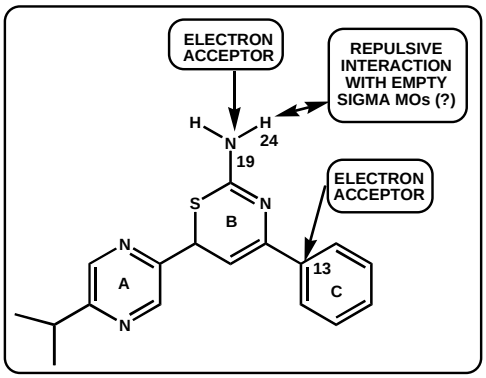

Figure 7: Partial 2D Pharmacophore for the Inhibition of Enterovirus 71

We have stated that "it is important to stress that our hypothesis covers multi-step (for example, in the n-th step molecules must cross a pore) and multimechanistic (for example, to cross the pore molecules must interact consecutively with j unknown sites) processes. *Therefore it seems logical to state that a necessary condition to obtain good structure-activity relationships is that all the steps and all the mechanisms inside each step must be the same for all the group of molecules under study*". It seems that for this case the results suggest that all the molecules have not the same action mechanism.

Discussion of the Results for the Inhibition of Coxsackievirus B3 (CVB3)

Table 6 shows that the importance of variables in Eq. 3 is F_{17} (LUMO+2)*> S_{18}^{E} (HOMO-2)*> S_{24}^{N} (LUMO+1)*> Q_2> Q_{16}> Q_{14}. The analysis of Eq. 3 shows that a high inhibitory activity is associated with large values for F_{17} (LUMO+2)*, large negative values for S_{18}^{E} (HOMO-2)*, large positive values for S_{24}^{N} (LUMO+1)* (if the numerical values of this index are positive), negative values for Q_2 and Q_{14}, and with positive values for Q_{16}. Atom 17 is a carbon in ring C (Figure 2). Table 10 shows that the three lowest empty local MOs have a π nature in all molecules. As a high inhibitory capacity is associated with large values for F_{17} (LUMO+2)*, it is suggested that this atom is acting as an electron acceptor. Atom 18 is a carbon in ring C (Figure 2). Table 10 shows that the three highest occupied local MOs have a π nature. Large negative values for S_{18}^{E} (HOMO-2)* are obtained by shifting upwards the energy of the corresponding eigenvalue, making this MO more reactive. This suggests that atom 18 is acting as an electron donor. Atom 24 is hydrogen (Figure 2). Table 10 shows that all MOs have a σ nature. For positive values of S_{24}^{N} (LUMO+1)* a high inhibitory activity is associated with large values for this index. Large values are obtained by shifting downwards the energy of the associated eigenvalue, making this MO more reactive. This means that this hydrogen atom is participating in a H-bond of the N…H…X kind. Atom 2 is a carbon in ring A (Figure 2). A high inhibitory activity is associated with a

negative net charge. The data employed in LMRA shows that atom 2 has a net charge of about -0.4. Therefore it is suggested that atom 4 is engaged in an electrostatic interaction with a counterpart having a positive net charge. Atom 16 is a carbon in ring C (Figure 2). A high inhibitory capacity is associated with positive values for its net charge. The analysis of the numerical values in the data matrix shows that the net charge of this atom is close to zero (-0.0x) in all molecules. Therefore a substitution producing positive net charges should help to enhance activity. This suggests that atom 16 is facing a negatively charged group. Atom 14 is a carbon in ring C (Figure 2). A high inhibitory activity is associated with negative values for its net charge. Almost net charges are negative in the data matrix employed for LRMA (one net charge is positive). Therefore we suggest that atom 14 is facing a positively charged group. All the suggestions are displayed in the partial 2D pharmacophore of Figure 8.

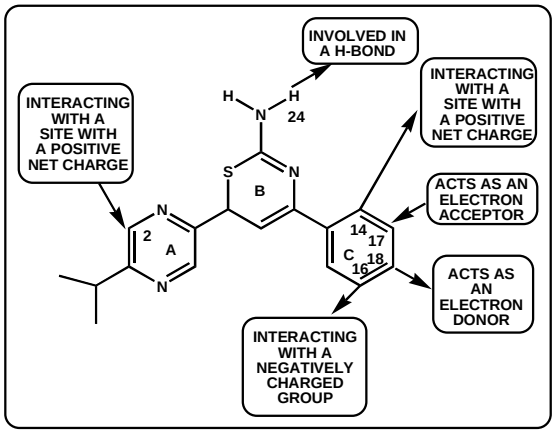

Figure 8: Partial 2D Pharmacophore for the Inhibition Coxsackievirus B3

In quantum chemical calculations many times some eigenvalues of empty MOs are negative. This is the reason why in our analysis we always stated that "*for a positive value of* $S_i^N(MO)$ *a high activity is associated with*", etc. The reader will easily verify that for negative values the analysis is exactly the same.

CONCLUSIONS

In conclusion, we have obtained at least two statistically significant equations relating the variation of the inhibitory activity against coxsackievirus B3 and H1N1 virus with the variation of the values of definite local atomic indices of a common skeleton. The results for Enterovirus 71 suggest that all the molecules studied here do not seem to have the same mechanism of action against this pathogen.

REFERENCES

1. Lin, C.; Sun, C.; Liu, X.; Zhou, Y., et al. Design, synthesis, and in vitro biological evaluation of novel 6-methyl-7-substituted-7-deaza purine nucleoside analogs as anti-influenza an agents. *Antiviral Research* **2016,** 129, 13-20.
2. Liang, J.; Cochran, J. E.; Dorsch, W. A.; Davies, I.; Clark, M. P. Development of a Scalable Synthesis of an Azaindolyl-Pyrimidine Inhibitor of Influenza Virus Replication. *Organic Process Research & Development* **2016,** 20, 965-969.
3. Drenichev, M. S.; Oslovsky, V. E.; Sun, L.; Tijsma, A., et al. Modification of the length and structure of the linker of N6-benzyladenosine modulates its selective antiviral activity against enterovirus 71. *European Journal of*

Medicinal Chemistry **2016,** 111, 84-94.

4. Chen, B.-L.; Wang, Y.-J.; Guo, H.; Zeng, G.-Y. Design, synthesis, and biological evaluation of crenatoside analogues as novel influenza neuraminidase inhibitors. *European Journal of Medicinal Chemistry* **2016,** 109, 199-205.
5. Tararov, V. I.; Tijsma, A.; Kolyachkina, S. V.; Oslovsky, V. E., et al. Chemical modification of the plant isoprenoid cytokinin N6-isopentenyladenosine yields a selective inhibitor of human enterovirus 71 replication. *European Journal of Medicinal Chemistry* **2015,** 90, 406-413.
6. Lin, M.-I.; Su, B.-H.; Lee, C.-H.; Wang, S.-T., et al. Synthesis and inhibitory effects of novel pyrimido-pyrrolo-quinoxalinedione analogues targeting nucleoproteins of influenza A virus H1N1. *European Journal of Medicinal Chemistry* **2015,** 102, 477-486.
7. Baltina, L. A.; Zarubaev, V. V.; Baltina, L. A.; Orshanskaya, I. A., et al. Glycyrrhizic acid derivatives as influenza A/H1N1 virus inhibitors. *Bioorganic & Medicinal Chemistry Letters* **2015,** 25, 1742-1746.
8. Qin, Y.; Lin, L.; Chen, Y.; Wu, S., et al. Curcumin inhibits the replication of enterovirus 71 in vitro. *Acta Pharmaceutica Sinica B* **2014,** 4, 284-294.
9. Jang, Y. J.; Achary, R.; Lee, H. W.; Lee, H. J., et al. Synthesis and anti-influenza virus activity of 4-oxo- or thioxo-4,5-dihydrofuro[3,4-c]pyridin-3(1H)-ones. *Antiviral Research* **2014,** 107, 66-75.
10. Dang, Z.; Jung, K.; Zhu, L.; Lai, W., et al. Identification and Synthesis of Quinolizidines with Anti-Influenza A Virus Activity. *ACS Medicinal Chemistry Letters* **2014,** 5, 942-946.
11. Torres, E.; Fernández, R.; Miquet, S.; Font-Bardia, M., et al. Synthesis and Anti-influenza A Virus Activity of 2,2-Dialkylamantadines and Related Compounds. *ACS Medicinal Chemistry Letters* **2012,** 3, 1065-1069.
12. Zhang, Z. L.; Sun, Z. J.; Xue, F.; Luo, X. J., et al. Design, synthesis and biological activity of some novel benzimidazole derivatives against Coxsackie virus B3. *Chinese Chemical Letters* **2009,** 20, 921-923.
13. Kuo, C.-J.; Shie, J.-J.; Fang, J.-M.; Yen, G.-R., et al. Design, synthesis, and evaluation of 3C protease inhibitors as anti-enterovirus 71 agents. *Bioorganic & Medicinal Chemistry* **2008,** 16, 7388-7398.
14. Wu, H.-M.; Zhou, K.; Wu, T.; Cao, Y.-G. Synthesis of Pyrazine-1,3-thiazine Hybrid Analogues as Antiviral Agent Against HIV-1, Influenza A (H1N1), Enterovirus 71 (EV71), and Coxsackievirus B3 (CVB3). *Chemical Biology & Drug Design* **2016,** 88, 411-421.
15. Gómez-Jeria, J. S. On some problems in quantum pharmacology I. The partition functions. *International Journal of Quantum Chemistry* **1983,** 23, 1969-1972.
16. Gómez-Jeria, J. S. Modeling the Drug-Receptor Interaction in Quantum Pharmacology. In *Molecules in Physics, Chemistry, and Biology*, Maruani, J., Ed. Springer Netherlands: 1989; Vol. 4, pp 215-231.
17. Gómez-Jeria, J. S.; Ojeda-Vergara, M. Parametrization of the orientational effects in the drug-receptor interaction. *Journal of the Chilean Chemical Society* **2003,** 48, 119-124.

18. Gómez-Jeria, J. S. *Elements of Molecular Electronic Pharmacology (in Spanish)*. 1st ed.; Ediciones Sokar: Santiago de Chile, 2013; p 104.

19. Gómez-Jeria, J. S. A New Set of Local Reactivity Indices within the Hartree-Fock-Roothaan and Density Functional Theory Frameworks. *Canadian Chemical Transactions* **2013,** 1, 25-55.

20. Gómez-Jeria, J. S.; Flores-Catalán, M. Quantum-chemical modeling of the relationships between molecular structure and in vitro multi-step, multimechanistic drug effects. HIV-1 replication inhibition and inhibition of cell proliferation as examples. *Canadian Chemical Transactions* **2013,** 1, 215-237.

21. Salgado-Valdés, F.; Gómez-Jeria, J. S. A Theoretical Study of the Relationships between Electronic Structure and CB1 and CB2 Cannabinoid Receptor Binding Affinity in a Group of 1-Aryl-5-(1-H-pyrrol-1-yl)-1-H-pyrazole-3-carboxamides. *Journal of Quantum Chemistry* **2014,** 2014 Article ID 431432, 1-15.

22. Gómez-Jeria, J. S.; Morales-Lagos, D. The mode of binding of phenylalkylamines to the Serotonergic Receptor. In *QSAR in design of Bioactive Drugs*, Kuchar, M., Ed. Prous, J.R.: Barcelona, Spain, 1984; pp 145-173.

23. Gómez-Jeria, J. S.; Morales-Lagos, D. R. Quantum chemical approach to the relationship between molecular structure and serotonin receptor binding affinity. *Journal of Pharmaceutical Sciences* **1984,** 73, 1725-1728.

24. Gómez-Jeria, J. S.; Cassels, B. K.; Saavedra-Aguilar, J. C. A quantum-chemical and experimental study of the hallucinogen (±)-1-(2, 5-dimethoxy-4-nitrophenyl)-2-aminopropane (DON). *European Journal of Medicinal Chemistry* **1987,** 22, 433-437.

25. Gómez-Jeria, J. S.; Ojeda-Vergara, M.; Donoso-Espinoza, C. Quantum-chemical Structure-Activity Relationships in carbamate insecticides. *Molecular Engineering* **1995,** 5, 391-401.

26. Gómez-Jeria, J. S.; Lagos-Arancibia, L.; Sobarzo-Sánchez, E. Theoretical study of the opioid receptor selectivity of some 7-arylidenenaltrexones. *Boletin de la Sociedad Chilena de Quimica* **2003,** 48, 61-66.

27. Gómez-Jeria, J. S. A DFT study of the relationships between electronic structure and peripheral benzodiazepine receptor affinity in a group of N,N-dialkyl-2- phenylindol-3-ylglyoxylamides (Erratum in: J. Chil. Chem. Soc., 55, 4, IX, 2010). *Journal of the Chilean Chemical Society* **2010,** 55, 381-384.

28. Barahona-Urbina, C.; Nuñez-Gonzalez, S.; Gómez-Jeria, J. S. Model-based quantum-chemical study of the uptake of some polychlorinated pollutant compounds by Zucchini subspecies. *Journal of the Chilean Chemical Society* **2012,** 57, 1497-1503.

29. Bruna-Larenas, T.; Gómez-Jeria, J. S. A DFT and Semiempirical Model-Based Study of Opioid Receptor Affinity and Selectivity in a Group of Molecules with a Morphine Structural Core. *International Journal of Medicinal Chemistry* **2012,** 2012 Article ID 682495, 1-16.

30. Alarcón, D. A.; Gatica-Díaz, F.; Gómez-Jeria, J. S. Modeling the relationships between molecular structure and inhibition of virus-induced cytopathic efects. Anti-HIV and anti-H1N1 (Influenza) activities as examples. *Journal of the Chilean Chemical Society* **2013,** 58, 1651-1659.

31. Gómez-Jeria, J. S. A quantum-chemical analysis of the relationships between hCB2 cannabinoid receptor binding

affinity and electronic structure in a family of 4-oxo-1, 4-dihydroquinoline-3-carboxamide derivatives. *Der Pharmacia Lettre* **2014,** 6. 95-104.

32. Gómez-Jeria, J. S. An Analysis of the Electronic Structure of an Imidazo[1,2-a]Pyrrolo[2,3-c]Pyridine series and their anti Bovine Viral Diarrhea Virus Activity. *British Microbiology Research Journal* **2014,** 4, 968-987.
33. Gómez-Jeria, J. S. toward Understanding the Inhibition of Vesicular Stomatitis Virus Replication in MDCK Cells by 4-Quinolinecarboxylic acid Analogues. A Density Functional Study. *Der Pharma Chemica* **2014,** 6, 64-77.
34. Gómez-Jeria, J. S. A Note on the Relationships between Electronic Structure and Inhibition of Chikungunya Virus Replication by a group of [1, 2, 3]Triazolo[4,5-d]pyrimidin-7(6H)-ones Derivatives. *Journal of Computational Methods in Molecular Design* **2014,** 4, 38-47.
35. Gómez-Jeria, J. S. A Density Functional Study of the Inhibition of the Anthrax Lethal Factor Toxin by Quinoline-based small Molecules related to Aminoquinuride (NSC 12155). *Research Journal of Pharmaceutical, Biological and Chemical Sciences* **2014,** 5, 780-792.
36. Muñoz-Gacitúa, D.; Gómez-Jeria, J. S. Quantum-chemical study of the relationships between electronic structure and anti influenza activity. 1. The inhibition of cytophatic effects produced by the influenza A/Guangdong Luohu/219/2006 (H1N1) strain in MDCK cells by substituted bisaryl amide compounds. *Journal of Computational Methods in Molecular Design* **2014,** 4, 33-47.
37. Muñoz-Gacitúa, D.; Gómez-Jeria, J. S. Quantum-chemical study of the relationships between electronic structure and anti influenza activity. 2. The inhibition by 1H-1, 2, 3-triazole-4-carboxamide derivatives of the cytopathic effects produced by the influenza A/WSN/33 (H1N1) and A/HK/8/68 (H3N2) strains in MDCK cells. *Journal of Computational Methods in Molecular Design* **2014,** 4, 48-63.
38. Gómez-Jeria, J. S.; Robles-Navarro, A. A theoretical study of the relationships between electronic structure and inhibition of tumor necrosis factor by cyclopentenone oximes. *Research Journal of Pharmaceutical, Biological and Chemical Sciences* **2015,** 6, 1337-1351.
39. Gómez-Jeria, J. S.; Robles-Navarro, A. A Density Functional Theory and Docking study of the Relationships between Electronic Structure and 5-HT_{2B} Receptor Binding Affinity in N-Benzyl Phenethylamines. *Der Pharma Chemica* **2015,** 7, 243-269.
40. Gómez-Jeria, J. S.; Robles-Navarro, A. A Quantum Chemical Study of the Relationships between Electronic Structure and cloned rat 5-HT_{2C} Receptor Binding Affinity in N-Benzylphenethylamines. *Research Journal of Pharmaceutical, Biological and Chemical Sciences* **2015,** 6, 1358-1373.
41. Gómez-Jeria, J. S.; Abarca-Martínez, S. A theoretical analysis of the cytotoxicity of a series of β-carboline-dithiocarbamate derivatives against prostatic cancer (DU-145), breast cancer (MCF-7), human lung adenocarcinoma (A549) and cervical cancer (HeLa) cell lines. *Der Pharma Chemica* **2016,** 8, 507-526.
42. Gómez-Jeria, J. S.; Castro-Latorre, P.; Kpotin, G. Quantum Chemical Analysis of the Relationships between Electronic Structure and Antiviral Activity against HIV-1 of some Pyrazine-1,3-thiazine Hybrid Analogues. *Der Pharma Chemica* **2016,** 8, 234-239.

43. Gómez-Jeria, J. S.; Cornejo-Martínez, R. A DFT study of the inhibition of human phosphodiesterases PDE3A and PDE3B by a group of 2-(4-(1H-tetrazol-5-yl)-1H-pyrazol-1-yl)-4-(4-phenyl)thiazole derivatives. *Der Pharma Chemica* **2016,** 8, 329-337.

44. Gómez-Jeria, J. S.; Latorre-Castro, P. On the relationship between electronic structure and carcinogenic activity in substituted Benz[a]anthracene derivatives. *Der Pharma Chemica* **2016,** 8, 84-92.

45. Gómez-Jeria, J. S.; Moreno-Rojas, C. A theoretical study of the inhibition of human 4-hydroxyphenylpyruvate dioxygenase by a series of pyrazalone-quinazolone hybrids. *Der Pharma Chemica* **2016,** 8, 475-482.

46. Gómez-Jeria, J. S.; Salazar, R. A DFT study of the inhibition of FMS-like tyrosine kinase 3 and the antiproliferative activity against MV4-11 cells by N-(5-(tert-butyl)isoxazol-3-yl)-N'-phenylurea analogs. *Der Pharma Chemica* **2016,** 8, 1-9.

47. Kpotin, G.; Atohoun, S. Y. G.; Kuevi, U. A.; Kpota-Hounguè, A., et al. A Quantum-Chemical study of the Relationships between Electronic Structure and Trypanocidal Activity against Trypanosoma Brucei Brucei of a series of Thiosemicarbazone derivatives. *Der Pharmacia Lettre* **2016,** 8, 215-222.

48. Kpotin, G. A.; Atohoun, G. S.; Kuevi, U. A.; Houngue-Kpota, A., et al. A quantum-chemical study of the relationships between electronic structure and anti-HIV-1 activity of a series of HEPT derivatives. *Journal of Chemical and Pharmaceutical Research* **2016,** 8, 1019-1026.

49. Robles-Navarro, A.; Gómez-Jeria, J. S. A Quantum-Chemical Analysis of the Relationships between Electronic Structure and Citotoxixity, GyrB inhibition, DNA Supercoiling inhibition and anti-tubercular activity of a series of quinoline–aminopiperidine hybrid analogues. *Der Pharma Chemica* **2016,** 8, 417-440.

50. Note. The results presented here are obtained from what is now a routinary procedure. For this reason, we built a general model for the paper's structure. This paper contains *standard* phrases for the presentation of the methods, calculations and results because they do not need to be rewritten repeatedly.

51. Frisch, M. J.; Trucks, G. W.; Schlegel, H. B.; Scuseria, G. E., et al. *G03 Rev. E.01*, Gaussian: Pittsburgh, PA, USA, 2007.

52. Gómez-Jeria, J. S. *D-Cent-QSAR: A program to generate Local Atomic Reactivity Indices from Gaussian 03 log files. v. 1.0*, v. 1.0; Santiago, Chile, 2014.

53. Gómez-Jeria, J. S. An empirical way to correct some drawbacks of Mulliken Population Analysis (Erratum in: J. Chil. Chem. Soc., 55, 4, IX, 2010). *Journal of the Chilean Chemical Society* **2009,** 54, 482-485.

54. Gómez-Jeria, J. S. Tables of proposed values for the Orientational Parameter of the Substituent. I. Monoatomic, Diatomic, Triatomic, n-CnH2n+1, O-n-CnH2n+1, NRR', and Cycloalkanes (with a single ring) substituents. *Research Journal of Pharmaceutical, Biological and Chemical Sciences* **2016,** 7, 288-294.

55. Gómez-Jeria, J. S. Tables of proposed values for the Orientational Parameter of the Substituent. II. *Research Journal of Pharmaceutical, Biological and Chemical Sciences* **2016,** 7, 2258-2260.

56. Statsoft. *Statistica v. 8.0*, 2300 East 14 th St. Tulsa, OK 74104, USA, 1984-2007.